DOI: 10.1111/cgf.15235
Pacific Graphics 2024
R. Chen, T. Ritschel, and E. Whiting
(Guest Editors)

COMPUTER GRAPHICS *forum*
Volume 43 (2024), Number 7

A Surface-based Appearance Model for Pennaceous Feathers

Juan Raúl Padrón-Griffe, Dario Lanza, Adrián Jarabo and Adolfo Muñoz

Universidad de Zaragoza-I3A, Spain

Figure 1: *A rendering of the wing of an* Amazon parrot. ***Left:*** *Bird model with a baked texture from a reference photograph of an Amazon parrot. Notice how the baked texture looks flat.* ***Center:*** *A surface-based rendering of the wing feathers, using a hair model [MJC*03] for representing the scattering from the microscopic structures of the wing, similar to previous approaches [HG19, BDSP22].* ***Right:*** *The same scene with feathers rendered using our model accounting for accurate masking and complex medulla using our BCSDF. Our far-field reflectance model represents more accurately the feather substructures and coloration mechanisms, given a closer appearance match with the baked texture overall appearance, including features such as the diffuse look of feathers, and the subtle goniochromatism due to visibility changes between barbs and barbules.*

Abstract

The appearance of a real-world feather results from the complex interaction of light with its multi-scale biological structure, including the central shaft, branching barbs, and interlocking barbules on those barbs. In this work, we propose a practical surface-based appearance model for feathers. We represent the far-field appearance of feathers using a BSDF that implicitly represents the light scattering from the main biological structures of a feather, such as the shaft, barb and barbules. Our model accounts for the particular characteristics of feather barbs such as the non-cylindrical cross-sections and the scattering media via a numerically-based BCSDF. To model the relative visibility between barbs and barbules, we derive a masking term for the differential projected areas of the different components of the feather's microgeometry, which allows us to analytically compute the masking between barbs and barbules. As opposed to previous works, our model uses a lightweight representation of the geometry based on a 2D texture, and does not require explicitly representing the barbs as curves. We show the flexibility and potential of our appearance model approach to represent the most important visual features of several pennaceous feathers.

CCS Concepts

• ***Computing methodologies*** → *Reflectance Modeling;*

1. Introduction

Feathers are the distinctive characteristic from birds, and are unique structures not shared with any other animal. They are crucial for flying, but also allow birds to control their body temperature, camouflage, and they are fundamental for communication in mating, aggression and dominance [HM06a].

The appearance of feathers is varied and rich, different among species, and is partially explained by the geometrical complexity of their structure at several levels: Each feather is composed of a central shaft, called the rachis, with its base (the calamus) is inserted to the skin. Serial fiber-like branches (barbs) emerge from both sides of the rachis. A second level of branching emerges from the barbs (the barbules), which in pennaceous feathers become attached to adjacent barbs, forming a flattened surface (the vane). Depending on the structure formed by barbules, feathers can have both pennaceous and plumulaceous sections. When barbules are interlocked to adjacent barbs, they create a tense and semi-rigid surface, characteristic of pennaceous areas. When barbules are loose, they form a fluffy, irregular volume typical of plumulaceous sections. Each of the barbs and barbules components possesses a scattering microstructure and nanostructure that greatly affects appearance: Different pigments (carotenoids and melanin) produce coloration through spectral absorption, while barbs have a multilayered structure with an inner scattering medulla which in some species have a quasi-ordered nanoscopic structure producing diffuse structural coloration. Photonic glass-like special nanostructures (e.g., grids of melanin rods) are responsible for the spectacular iridescent patterns in feathers of birds such as the peacock or the bird of paradise. It is only the aggregated behavior of light-matter interactions at these scales that produce the complex appearance of feathers. Beyond direct applications for traditional computer graphics applications, the appearance of feathers has also been studied for ornithology [HM06a], paleontology for color reconstruction of extinct dinosaur feathers [ZKO*10], or fabrication of new biomimetic materials [FWLQ23].

Compared to other biological appearances such as skin [Sta01, DWd*08, IGAJG15], hair [MJC*03] or fur [YTJR15], rendering of feathers, and in particular of pennaceous feathers, is a relatively unexplored area in computer graphics, with some notable exceptions that either oversimplify the appearance [Str03], bake it in a Bidirectional Texture Function (BTF) [CXGS02], focus on specific bird species [HMC*22], or use expensive curve-based representations for the barbs with simplified fiber scattering functions [BDSP22]. While modeling the barbs as curves [HMC*22, BDSP22] is flexible, allows for a very fine-detailed representation of the feathers, and explicitly accounts for geometric effects such as visibility, it might become very expensive when representing many feathers, quickly becoming impractical in most applications.

In this work we propose a far-field surface-based appearance model for pennaceous feathers, that encodes the geometric complexity of the feather by using lightweight textures, and that it is able to correctly predict the geometric attenuation that so far could only be modeled with explicit curve-based feathers. At the core of our model is a new Bidirectional Scattering Distribution Function (BSDF) that accounts for the scattering of barbs and barbules stochastically, based on their density and orientation, as well as their relative visibility. Inspired by previous works [dFH*11, HMC*22, BDSP22], we model the individual scattering of both barbs and barbules using a fiber-based Bidirectional Curve Scattering Distribution Function (BCSDF). However, as opposed to these previous works, our BCSDF accounts for the ellipticity of the fibers and the effect of the internal non-centered scattering medulla, which are crucial for the appearance of most feathers, specially bright colored feathers.

We demonstrate our work representing a wide baseline of feather appearances, including pure white feathers, blue feathers due to diffuse structural coloration, or feathers with color resulting from hybrid coloration. None of these can be represented with previous models. In particular, our contributions are:

- A flexible BSDF that models the far-field appearance of non-iridescent pennaceous feathers,
- an elliptical BCSDF that generalizes previous curve scattering models by accounting for both elliptical cross-section and the presence of a non-centered scattering medulla,
- and an analytic masking term that combines the relative contribution between barbs, barbules, and transparency based on their differential projected areas.

Our source code, scenes and additional examples are available at the project website https://graphics.unizar.es/projects/FeathersAppearance_2024/.

2. Related Work

Feather appearance The modeling of the appearance of feathers remains a relatively unexplored area of research. Most of previous works focus on the modeling of the geometry of the feather, defining parametrical models that simulate the geometrical structure of each feather. Rachis and barbs have been modeled using NURBS and structured in feathers using L-Systems [CXGS02], and Bezier curves both for the structure of feathers and for individual barbs [CXGS02, Str03]. Data-driven approaches based on images of real feathers have been able to model not only rachis and barbs but also barbules [BP19, BP21a]. Lately, a generative algorithm based on the biological growth of feathers has been able to model realistic feathers with three-dimensional features [ZK20]. These works are orthogonal to our work, and could be used for generating our surface-based representation described in Section 6.2.

Regarding appearance modeling, Chen et al. [CXGS02] proposed to use data-driven appearance based on BTFs, which require capturing the feather and has limited angular resolution. Haapaoja and Genzwürker [HG19] and Leaning and Fagnou [LF10] modeled the scattering from barbs using a hair BCSDF [MJC*03], but ignored the scattering from barbules. Harvey and colleagues [HBM13] proposed a data-driven model for the African Emerald Cuckoo, based on measured data and expensive wave simulations. Closest to our work, Huang et al. [HMC*22] and Baron et al. [BDSP22] accounted for the scattering of both barbs and barbules, with the former modeled statistically. In particular, Huang and colleagues [HMC*22] focused on the iridescent appearance of plumaceous rock dove neck feathers, proposing a BSDF for explicit barbs that simulates barbule scattering using a microfacet-like model with thin-film iridescence, while accounting for inter-barbule masking. In contrast, our work focuses on general non-iridescent pennaceous feathers. Baron et al. [BDSP22] focus on general feathers, representing barbs as curves where the BCSDF combines the scattering of both barbs and barbules, using Marschner's hair model [MJC*03]. In contrast, our model is a general, compact surface-based representation for pennaceous feath-

ers, where the scattering of both barbs and barbules is modeled using a new BCSDF that accounts for elliptical cross-sections and inner scattering medulla allowing to represent a wider range of light-matter interactions occurring at barb and barbule scale.

Microstructure-based surface scattering Statistical aggregated representations of the detail at the microscopic level are the common choice for representing the scattering of small features. The most common approaches are microfacet models [CT81, WMLT07, JHY*14] that represent rough surfaces as statistical aggregates of tiny planar surfaces, generally assuming uncorrelation for computing the geometric attenuation [Hei14]. Other approaches assume other microscopic scatterer shapes, including spherical scatterers [d'E21], bumps and cavities [MDG00], scratches [BPMG04], or micrograins [LRPB23], which allow computing specific geometric attenuation terms. Closer to our work, far-field models for woven cloth [IM12, SBDDJ13] assume a particular structure between perpendicularly interwoven yarns with fiber-like scattering; this structure allows to derive a closed-form masking functions between the different yarns. Our model also models the scattering of each component using a BCSDF, but incorporates the additional complexity of the multiscale structure of barbs and barbules.

Scattering from fibers Cylinder-based scattering models based on the BCSDF have been proposed for realistic human hair for circular [MJC*03, dFH*11, CBTB16] and elliptical fiber cross sections [KM17, BP21b, HHH22]. Follow-up work extended hair models to fur, by adding a scattering medulla crucial for the soft look of fur [YTJR15, YJR17]. Cloth fibers and yarns have also been represented using the BCSDF, either measured with gonioreflectometers [SBDDJ13] or simulated from the microgeometry of the fibers [ACG*17, XWM*20]. To reduce the cost of rendering individual fibers, aggregation techniques have been proposed to approximate the aggregated appearance in fur [ZZW*22] and cloth fibers [KZP*24]. Our model for fiber scattering builds upon these models, but generalized to the specific structure of the barbs and barbules that compose the feather, combining elliptical cross-sections with a non-centered scattering medulla.

3. On the appearance of feathers

The appearance of feathers is the result of a complex light-matter interactions at multiple scales. It depends on both internal structure and chemical composition. The structure and type of feather affect its appearance at a high level, while the chemical composition and micro-nanoscale structure fundamentally change its coloration, opacity and reflectance.

3.1. Structure

Although feathers are incredibly diverse in shape and size, they are all composed primarily of keratin, a protein present in all epidermal structures of all vertebrates. Unlike the epidermal structures of mammals (e.g. hair or nails) whose main component is α-*keratin*, the structures of birds and reptiles are based on β-*keratin*, which makes them more rigid. This protein is present in all the epidermal structures of birds (beak, claws, feathers ...) in different ways depending on the corresponding biological functions. The microstructure of β-*keratin* on feathers is, biomechanically, more flexible, providing unique properties required for flight [PZS*19].

Feather structure. The main components of a typical feather consist of a long and central axis in which two parts are considered: the lower and wider part, which is inserted on the skin (**calamus**) and the rest of the axis (**rachis**). On both sides of the rachis, the **vane** grows as a lamina and is formed by **barbs**, which grow along the entire rachis in a branching manner. Each barb consists of a central axis of tens of microns (**ramus**), which branches out on both sides in rows of hundreds of microscopic-sized **barbules** (**proximal** and **distal**), coupled by hooklets [HBM13, SWEM17]. Barbules are up to an order of magnitude smaller than barbs [HMC*22], and branch from their respective barb, often in a $\phi_{bb} = 45^\circ$ angle to maximize their overlap, favoring the grip of the hooklets [EHR95]. This ramification results in features at multiple scales (see Figure 2). Previous work [BP21a] collected data from ornithological studies including barb density, barb angles or barbule length. There is an important variety of geometric structures and configurations for barb and barbules depending on the bird species and even sex [MSV*21]. For instance, some cross sections such as the barbule cross-section shapes of a peacock tail feather (see Fig. 3 [FS20]) or a Lawes' parotia breast feather (see Fig. 3 [SLMO11]) with ridged forms. Nevertheless, the cross sections of these internal structures tend to be elliptical (see Fig. 4 [MSV*21]) as we show in the Scanning electron microscopic (SEM) images of the kingfisher feather Figure 3 (c), with eccentricity up to 6 depending on the specie [IDS18]. For this reason, as previous work [HMC*22], we approximate these cross sections as ellipses.

Feather taxonomy. Feathers can be classified according to size, shape, and type [SH02]. One of the main features is the type of vane: **plumulaceous** (fuffy, diffuse and soft) or **pennaceous** (mostly flat, firm and rigid, due to interlocked barbules). In this work, we focus on pennaceous feathers, as these ones can be modeled with a BSDF over a surface that represents the vain. A surface representation allows us to encode the feathers as texture, a representation quite effective especially for far field scenarios. On the other hand, plumulaceous feathers require the modeling of individual barbs over a volume. For a further discussion about the feather taxonomy and potential representations, we refer the reader to previous work specialized on feather geometry [SH02, BP19].

3.2. Coloration

Feathers combine pigmentation and structural coloration to create extraordinary and diverse colors, more than for any mammal and most vertebrates [HM06b]. The colors of the bird feathers play an essential role in a variety of biological functions such as camouflage, visual signaling or mating [RPD*14].

Pigmentation. Pigment-based coloration is the most common in vertebrates and is caused by the absorption of certain wavelengths as light traverses the pigments (Figure 4, left). Pigments are molecules that absorb and reflect each of the wavelengths of light, hence they can be associated with a particular color. These pigments are deposited between the keratin sheets that make up the barbs, barbules and rachis [RPD*14]. The most prevalent pigments in feathers are based on melanin, which is responsible for a wide

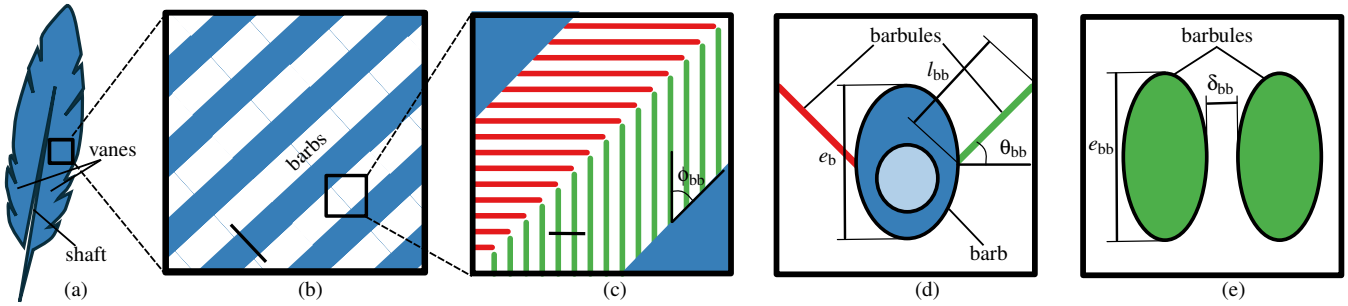

Figure 2: *(a) The appearance of the feather's vane (a) depends on its underlying structure. (b) Parallel barbs emerge from the rachis. (c) Each barb branches into two sets of barbules, proximal and distal. (d) Barbs are modeled as infinite cylinders with elliptical cross section, with an inner medulla with elliptical cross section. Barbules' thickness is negligible so at this level they are modeled as the plane in which they lie. (e) At a smaller scale, barbules are also cylinders with elliptical cross section, and can occlude each other. They have some spacing between them that at a larger level is treated as partial transparency that is considered at a larger (barb) scale. The microgeometrical parameters of our model are also represented.*

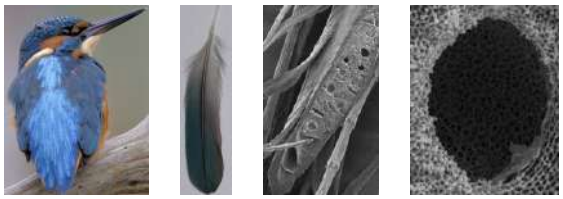

Figure 3: *(a) Kingfisher (Alcedo atthis). (b) Blue tail feather of a kingfisher. (c) Top-view SEM of a sectioned barb of the feather with several barbules (50 μm). (d) Cross section SEM of a cut vacuole and the surrounding spongy structures (2 μm). Notice the elliptical shape of the barb cross section and the presence of the medulla with an internal spongy structure (Source [STLW11]).*

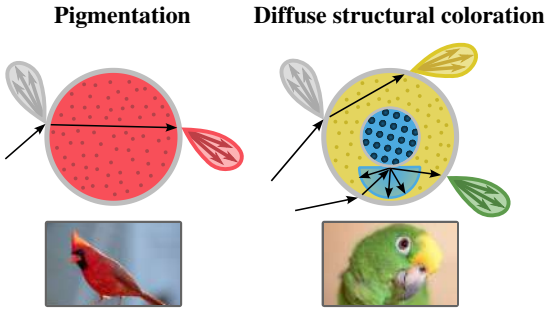

Figure 4: *Cross-section fiber schematic of the coloration mechanisms in feathers supported by our appearance model.* ***Left****: Pigments-based coloration where some wavelengths are absorbed by the pigment granules located in the keratin matrix.* ***Right****: Diffuse structural coloration, where in addition to pigmentation, the medulla scatters colored light due to interference.*

range of colors, usually brown, gray and black tones [SD17]. or carotene, that produce more vivid colors such as reds, yellows, and oranges [RPD*14, SD17, WDM*12, MPLS*12].

Structural coloration. The structural coloration of bird feathers is caused by the scattering and interference of light with the feather nanoscopic structure [FWS19]. This coloration does not depend entirely on absorption, but on the way the structure of the feathers disperses certain wavelengths. One source of such structural coloration are specialized keratin structures in the medulla of the barbs, which create a pseudo-ordered matrix of keratin and air bubbles, known as the spongy layer (Figure 3, d). These lead to non-iridescent tones of blue, violet and UV [Pru99], as illustrated in Figure 4, although in some cases they generate partial iridescence for highly directional illuminations [STLW11], which disappears with lower frequency illuminations. We account for this effect with a diffuse medulla, that approximates the backscattering given by constructive interference in such quasi-ordered structures [NLS*10].

Hybrid coloration Some colors such as blues, greens and purples are created by the combination of the structure and the pigments. For instance, the green color is usually a combination of yellow pigmentation with a blue structural color [MPLS*12] (Figure 4, right). Feather goniochromatism can occur from the partial occlusions between barbs and barbules of different colors at different view orientations, which we model through a masking expression.

4. Overview

The scattering of each barb and barbule is modeled as a BCSDF [ZW07], which assumes that each fiber is an infinite locally-straight cylinder (Section 5). The aggregated appearance comes from combining such BCSDFs in their local frame, as obtained from the tangent map and the geometrical parameters of the BSDF. The scattering radiance from each BSDF is weighted based on the corresponding projected visible area as defined by our masking term (Section 6). Masking is computed on the fly when our feather BSDF is evaluated or sampled. . The structural and optical parameters of our model can affect either particular BCSDFs (for barbs or barbules), the global BSDF or both. These are summarized in Table 1 and some of them are illustrated on Figure 2. The feather's geometry is encoded in a 2D texture applied on a plane or

curved plane: The red channel encodes the barb orientation and the blue channel stores a flag identifying rachis, vane, and background. We manually designed the texture to roughly match the feathers' silhouette based on feather photographs. More details about the authoring process can be found in the supplemental document.

Parameter	Definition
β_m	Longitudinal roughness of cortex
β_n	Azimuthal roughness of cortex
$\sigma_{c,a}$	Absorption coefficient in cortex
η_c	Refractive index of cortex
a_c	Cortex semi-major axis
b_c	Cortex semi-minor axis
$\sigma_{m,a}$	Absorption coefficient in medulla
d_m	Diffuse reflectance of medulla
η_m	Refractive index of medulla
a_m	Medulla semi-major axis
b_m	Medulla semi-minor axis
$(c_{m,a}, c_{m,b})$	Medulla center (w.r.t. to cortex center)
ϕ_b	Azimuthal barb angle
ϕ_{bb}	Azimuthal barbule angle
θ_{bb}	Longitudinal barbule angle
δ_{bb}	Barbule separation
l_{bb}	Barbule length

Table 1: *Parameters of our Feather BSDF. The angles (ϕ_b, ϕ_{bb}, θ_{bb}) are expressed in degrees. The sub-index b refers to barbs, while the bb refers to barbules. l_{bb} and δ_{bb} are measured in number of barb and barbules per length unit respectively. The eccentricity for e_b and barbules cross section e_{bb} are computed from the cortex axes a_c and b_c of the corresponding internal structure.*

We introduce the following assumptions:

1. No wave-optical effects are present between barbs and barbules, and all scattering can be considered in the ray-optics regime. Wave optics is particularly significant for iridescent feathers such as the hummingbird and peacock feathers. In this work, we focus on pennaceous non-iridescent feathers which extend a large group of feathers.
2. As previous work [HMC*22], we assume an elliptical cross-section of both barbs and barbules. While this is mostly accurate for barbs, barbules come in different shapes, which are specially relevant for iridescent feathers [HBM13].
3. Multiple scattering only occurs inside the fibers (accounted by the BCSDF), but not among barbs and barbules on the same surface. When rendering (path tracing), multiple scattering emerges from the interactions among different surfaces.
4. We assume that shadowing has a negligible effect, which allows our model to compensate for energy loss due to the lack of multiple scattering among barbs and barbules.
5. The microstructure of the feather's vane is locally regular: In a differential surface patch, barbs are parallel, proximal barbules are parallel and distal barbules are parallel. This removes the need of explicitly modeling the geometry of all barbs and barbules.

In the following, we first define our new BCSDF that supports some of the observed structural properties of both barbs and barbules; then, we define our surface BSDF that leverages the BCSDFs for modeling the aggregated scattering at the feather's vane.

5. Scattering from barbs and barbules

Here we model the scattering of the main individual components of the feather as a BCSDF. Then, we describe our structural model for barbs and barbules; then, we describe the BCSDF used for modeling the three of them. Following the formulation from [MJC*03], we define the far-field BCSDF in polar coordinates, as

$$S(\phi_i,\theta_i,\phi_o,\theta_o,h^-,h^+) = \frac{D(\phi_i)\cos(\theta_i)^{-2}}{h^+-h^-}\int_{h^-}^{h^+} S(\phi_i,\theta_i,\phi_o,\theta_o,h)dh, \tag{1}$$

where (ϕ_i,θ_i) and (ϕ_o,θ_o) parametrize in polar coordinates the incident and outgoing direction respectively, $D(\phi_i)$ is the projected fiber width on the incident direction, $\cos(\theta_i)^{-2}$ accounts for the projected solid angle of the specular cone, h^- and h^+ parametrize the limits of the visible fiber diameter (for a fully visible fiber, $h^-=-1$ and $h^+=1$), and $S(\phi_i,\theta_i,\phi_o,\theta_o,h)$ is

$$S(\phi_i,\theta_i,\phi_o,\theta_o,h) = \iint \mathcal{S}(\phi_i,\theta_i,\Phi,\Theta,h)G_M(\Theta-\theta_o|\beta_m) G_N(\Phi-\phi_o|\beta_n)\cos(\Theta)d\Theta d\Phi, \tag{2}$$

where $G_M(\Delta\theta|\beta_m)$ and $G_N(\Delta\phi|\beta_n)$ are longitudinal and azimuthal Gaussian detector functions respectively [dFH*11], that regularize the scattered field accounting for surface roughness (parametrized by β_m and β_n, respectively). Finally, $\mathcal{S}(\phi_i,\theta_i,\Phi,\Theta,h)$ models the transfer function inside the fiber, defined as the integral of paths starting at (ϕ_i,θ_i,h) and outgoing at direction (Φ,Θ) following the path integral [Vea97]

$$\mathcal{S}(\phi_i,\theta_i,\Phi,\Theta,h) = \int_\Omega f(\mathbf{x})d\mu(\mathbf{x}), \tag{3}$$

with Ω the space of paths $\mathbf{x}$ that start at (ϕ_i,θ_i,h) and end at (Φ,Θ), and $\mu(\mathbf{x})$ the measure of the integral. For purely absorbing fiber, the space of paths starting at (ϕ_i,θ_i,h) is singular specular path, and thus $\mathcal{S}(\phi_i,\theta_i,\Phi,\Theta,h)$ is a sum of impulse functions, one per bounce inside the fiber, with amplitude the attenuation at each bounce.

5.1. Fiber models

We do not model the scattering from the rachis as a BCSDF; instead, we assume that the diffuse scattering medulla is dominant and model it as a colored diffuse surface.

We model **barbs** and **barbules** as cylindrical β-keratin cortex with elliptical cross section, with axes a_c and b_c. The interface is a rough dielectric, with roughness modeled as azimuthal and longitudinal 1D Gaussian detectors as described above), and index of refraction η_c. The β-keratin hosting medium is filled with absorbing pigments, leading to an exponential transmittance as predicted by Beer-Lambert law.

Additionally, the barb contains a **medulla**. As opposed to hair and fur models [YTJR15], the medulla is generally not aligned with the cortex center, nor have the same eccentricity. We thus do not model cortex and medulla as concentric cylinders, but instead allow the medulla to position freely inside the cortex, with axes a_m and b_m and center $(c_{m,a},c_{m,b})$. As anticipated before, we approximate the

reflectance of the medulla as a diffuse surface. The albedo ranges from white (when there is no spongy layer) to blue, representing the non-iridiscent coloration of the spongy layer (as described before). We use measured reflectances for the blue tint, from the work by Noh et al. [NLS*10].

5.2. Rendering

Our model for barbs and barbules involves elliptical cross sections and a diffuse medulla (for the case of barbs), so our solution is not simple enough for a closed-form expression for Equation (1), specially as we account for higher-order bounces inside the fiber. Thus, we need to solve the integral numerically. Inspired on the work of Chiang et al. [CBTB16] we leverage the stochastic nature of modern renderers and compute the nested integrals in Equation (1) with a Monte Carlo estimate.

We implement a stochastic Monte Carlo-based path tracer from which we obtain a set of fixed number of *lobes*. In our experiments, we observed that five lobes seem to be accurate enough as we shown in Figure 13. Each of these lobes consists of an outgoing radiance value (throughput) associated to an outgoing direction. Each interaction with each dielectric interface (cortex) deterministically generates two rays: one exiting the cortex, which we store as a lobe, and one entering the fiber, which keeps interacting and generating lobes until the final number is reached. The stochastic exploration of those sets of lobes comes from the integration variable of Equation (1) h and, in the case of barbs, the interactions with the medulla, from which we generate new rays using cosine sampling.

For **evaluating** the BCSDF, we go through all the lobes, evaluating the Gaussian detector functions $G_M(\Theta-\theta_o|\beta_m)$ and $G_N(\Phi-\phi_o|\beta_n)$ (see Equation (2)) for the direction of the lobe (Θ,Φ), and $\mathcal{S}(\phi_i,\theta_i,\Phi,\Theta,h)$ is a one-sample estimate of the lobe's throughput. For **sampling** the BCSDF, we follow a strategy similar to previous works [dFH*11] where we build a discrete pdf where the accumulated throughput of each lobe corresponds to the probability of such lobe.

6. Our surface appearance model

As opposed to previous works [HMC*22] that explicitly model the rachis and barbs as curves, we represent feathers using a surface-based representation, where the geometry explicitly model the rachis and vanes, while barbs and barbules in the vanes are modeled as microgeometry, using a BSDF defined in the local coordinate system of the barbs. As described before, we encode the feather parameters in texture space, using a mask to distinguish between rachis and vanes, and defining the local tangent direction on the surface using a rotation angle. This removes the need of modeling explicit geometry of the feather, resulting in a compact representation.

Our BSDF $f_s(\omega_i,\omega_o)$ is a linear combination of four different components: barb BCSDF S_b and proximal and distal barbules BCSDFs S_bb modeled using Equation (2) (below in Cartesian coordinates instead of polar), and transmittance through the vane. The BSDF is defined in the local coordinates of the barb, defined by the normal of the surface and the barb's tangent direction, following

$$\begin{aligned} f_s(\omega_i,\omega_o) = \Big[& w_\mathrm{b}(\omega_o)\, S_\mathrm{b}\left(\omega_i,\omega_o,h_\mathrm{b}^-(\omega_o),h_\mathrm{b}^+(\omega_o)\right) G(\omega_i) \\ & + w_\mathrm{bp}(\omega_o)\, S_\mathrm{bb}\left(\mathbf{T}_\mathrm{bp}\omega_i,\mathbf{T}_\mathrm{bp}\omega_o,h_\mathrm{bp}^-(\omega_o),h_\mathrm{bp}^+(\omega_o)\right) G(\mathbf{T}_\mathrm{bp}\omega_i) \\ & + w_\mathrm{bd}(\omega_o)\, S_\mathrm{bb}\left(\mathbf{T}_\mathrm{bd}\omega_i,\mathbf{T}_\mathrm{bd}\omega_o,h_\mathrm{bd}^-(\omega_o),h_\mathrm{bd}^+(\omega_o)\right) G(\mathbf{T}_\mathrm{bd}\omega_i) \\ & + w_\mathrm{t}(\omega_o)\,\delta(1-\omega_i\cdot\omega_o)\Big] |\omega_i\cdot\mathbf{n}|^{-1}, \end{aligned} \tag{4}$$

where $\mathbf{n}$ is the surface normal, $w_\mathrm{b}(\omega_o)$, $w_\mathrm{bp}(\omega_o)$ and $w_\mathrm{bd}(\omega_o)$ model the projected area of the barb, proximal barbule and distal barbule as viewed from ω_o, respectively, $w_\mathrm{t}(\omega_o)=1-(w_\mathrm{b}(\omega_o)+w_\mathrm{bp}(\omega_o)+w_\mathrm{bd}(\omega_o))$ is the amount of transparency, $\delta(\cdot)$ is the Dirac delta distribution, $\mathbf{T}_\mathrm{bp}$ and $\mathbf{T}_\mathrm{bd}$ transform the coordinate system to the frame of proximal and distal barbules, according to their rotation $\phi_\mathrm{bb}=45^\circ$ and inclination θ_bb (parameter of our model), and $G(\omega_i)=\cos(\theta_i)$ the foreshortening over the fiber. The integration ranges for the corresponding BCSDFs are $[h_\mathrm{b}^-(\omega_o),h_\mathrm{b}^+(\omega_o)]$, $[h_\mathrm{bp}^-(\omega_o),h_\mathrm{bp}^+(\omega_o)]$ and $[h_\mathrm{bd}^-(\omega_o),h_\mathrm{bd}^+(\omega_o)]$. Both the projected areas $w(\omega_o)$ and the integration ranges (h^-,h^+) for barb and barbules are given by our masking term (Section 6.1). Finally, note that for all BCSDFs we set the fiber width $D=1$, since it is accounted for by the projected areas w_b, w_bp and w_bd, respectively.

6.1. Masking

We do not explicitly model the feather's microgeometry, but instead devise an analytical masking expression that analyzes the visibility among its components. Our masking expression works at two different scales: barbs and barbules. The critical insight for developing our masking components is that, at their respective local coordinate systems, all the microgeometrical elements are either ellipses or segments. Both are governed by implicit and parametric equations from which we can derive both projected areas within a parameter subrange. Furthermore, instead of stochastically explore the visibility, as the work by [HMC*22] does for barbules, we find analytical points that correspond to visibility discontinuities by tracing 2D rays at the analytical boundaries, and from the arcs/segments between the corresponding intersections we calculate projected areas.

We name $\omega_o'=\{\omega_{ox}',\omega_{oy}'\}$ the two-dimensional direction in the local coordinate space (the longitudinal dimension is ignored) after transforming ω_o. For an ellipse (representing barb or barbule) with center $\mathbf{c}=\{c_x,c_y\}$ and axes a_x and a_y the visibility discontinuities as given by that ellipse are its tangent points, obtained as:

$$\mathbf{p}_{t0}=\begin{pmatrix}c_x+a_x\cos(\alpha)\\ c_y+a_y\sin(\alpha)\end{pmatrix} \qquad \mathbf{p}_{t1}=\begin{pmatrix}c_x+a_x\cos(\alpha+\pi)\\ c_y+a_y\sin(\alpha+\pi)\end{pmatrix} \tag{5}$$

where $\alpha=\tan^{-1}\left(\frac{-a_y\omega_{ox}'}{a_x\omega_{oy}'}\right)$.

For barbs, the corner among barbule segments $\mathbf{p}_c$ represents a visibility discontinuity too. These visibility boundary points are the origin of 2D rays traced towards the rest of the elements of the microgeometry at their specific scale. Once the visibility among the different geometrical elements, projected areas towards ω_o' are calculated through a simple cosine for the case of segments and for

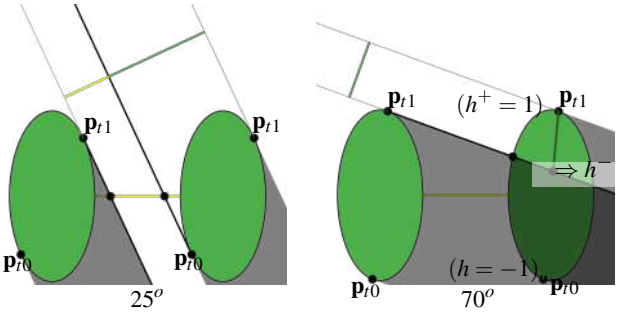

Figure 5: ***Masking between two barbules at different view inclinations.*** *Barbules (and their projected area) are marked in green. The barbule separation and traced rays are shown as yellow and black segments respectively. We first trace a ray from the tangent point $\mathbf{p}_{t1}$, generating two cases: If it intersects the other ellipse (70^o case) we need to intersect the ellipse's diameter to identify $\mathbf{p}_d$ and therefore h^-. The separation (transparency) cannot be seen ($w'_{bb} = 1$). If it does not intersect the other ellipse (25^o case) then we need to intersect the separation segment with two tangent rays. We then calculate the local barbule weight w'_{bb} from the projected areas a_{bb} and a_s.*

the case of ellipses, its projected area A is:

$$A(u_0,u_1) = \omega'_{ox}a_y(\sin(u_0) - \sin(u_1)) + \omega'_{oy}a_x(\cos(u_1) - \cos(u_0)) \tag{6}$$

where u_0 and u_1 are the starting and ending parameters from the ellipse's parametric equation, obtained by inverting the parametric equation for the intersection (visibility boundaries) points. The derivation of this inversion and of Equation (6) can be found in the supplemental material.

Barbule masking At a smaller scale, which we call *barbule masking* we align the reference frame at the local barbule frame. Given the cross section of barbules (ellipses) and a separation among them, we obtain the ratio between barbule visibility and transparency, as well as the casting segment range for the barbule (see Figure 2 and Figure 5). This is done at the local coordinate system of proximal and distal barbules, and the result is used for the larger-scale barb masking. Note that previous work [HMC*22] models this masking term stochastically, and not analytically.

We explicitly model two barbules as ellipses while the separation between them is a segment (as represented in Figure 5). The barbule model parameters are, for reducing the number of parameters, the barbule axis ratio e_{bb} and the relative barbule separation δ_{bb}. We trace 2D rays from a tangent point at each ellipse towards each other and the separation segment. If there is occlusion between ellipses (ray has intersected) the lower limit of the integration range h^- ($h^-_{\text{bp}}(\omega_o)$ or $h^-_{\text{bd}}(\omega_o)$) require tracing the same ray again towards the segment between $\mathbf{p}_{t0}$ and $\mathbf{p}_{t1}$ that represents the diameter of the ellipse. h^- is the parameter of the parametric equation of this diameter at the intersection point $\mathbf{p}_d$ (if there is no intersection, $h^- = 1$. The other integration range limit is $h^+ = 1$. These geometrical elements can be visualized on Figure 5. This barbule masking term is applied twice, for both proximal and distal barbules, obtaining h^-_{bp}, h^+_{bp}, h^-_{bd}, h^+_{bd} and, from the projected areas, local weights w'_{bp} and w'_{bd}. As barbules are separated, there is also the possibility of local transparency with weights $1 - w'_{\text{bp}}$ and $1 - w'_{\text{bd}}$, respectively.

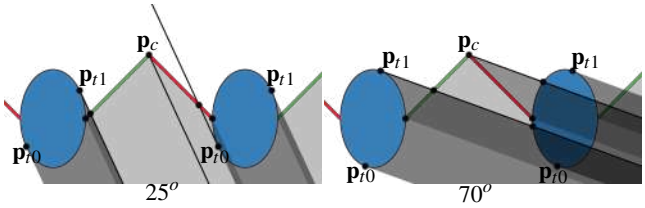

Figure 6: ***Cross section of barbs, representing the masking between barbs at two different view inclinations.*** *Barbules (in red and green, respectively) are partially transmitting, depending on the view direction at their particular local coordinates (see Figure 5), while barbs (in blue) are considered to be opaque. Depending on the view direction, each element (barbs and barbules) totally or partially occludes the rest. The limits of such occlusions are identified by tracing 2D rays (marked in black). By considering all the particular intersection ranges we obtain the weights.*

Barb masking At the upper scale, *barb masking*, we align the reference frame to the barb local frame. Hence the cross section of the barb is an ellipse, and the cross sections of the barbules are two segments (distal and proximal), with partial transparency obtained from the barbule masking component. Here, we compute the visibility ratios between barbs, barbules, and transmittance (see Figure 6 and Figure 2, d). Note that previous work [HMC*22] does not provide a masking term that accounts for barbs and need to explicitly model the geometry of each individual barb.

Parameters are also relative with respect to the horizontal size of the barb, and include axis ratio e_{b}, barbule length l_{bb} and barbule inclination θ_{bb}. From these we obtain a representation of the microgeometry with two ellipses (barbs) and two pairs of segments (barbules). We trace rays from the visibility discontinuity points $\mathbf{p}_{t0}$, $\mathbf{p}_{t1}$ and $\mathbf{p}_c$ towards the rest of geometrical elements (segments and ellipses) and, from the ranges between intersection points, calculate the projected areas as before. Each interval correspond to total or partial occlusions (at this scale, barbules are partially transparent) so each projected area must be multiplied by $1 - w'_{\text{bp}}$ if it is occluded by the proximal barbule and by $1 - w'_{\text{bd}}$ if it is occluded by the distal barbule. We combine all projected areas and obtain w_{b}, w_{bp} and w_{bd}. We also obtain h^-_{b} and h^+_{b} using the same procedure than for barbules. A detailed step-by-step procedure for obtaining these masking terms can be found as supplemental material.

6.2. Rendering

For evaluating the BSDF as described by Equation (4), we simply calculate the weights from the masking expression and then evaluate the corresponding BCSDFs at their local coordinate systems. For sampling it, we use a discrete distribution, similar to previous work [BDSP22] with four possible events (hit barb, hit proximal/distal barbules and delta transmittance) whose probabilities come from weights obtained from the analytical masking expression. The selected event is then sampled, deterministically if it is a

Figure	# Feathers	Resolution	Spp	Time
Figure 7	2500	512×256	1024	2.2 min
Figure 8	82	730×420	256	4.4 min
Figure 10	496	512×512	256	1.5 min
Figure 11	1	256×512	1024	1.5 min

Table 2: *Rendering time for different scene complexities: single feather, feather pelt, feather wing and feather ball.*

delta transmittance or by using the BCSDF sampling routine of the specific fiber otherwise.

7. Analysis and Results

In this section, we perform several experiments to show the capability of our feather BSDF, formal validation of our analytical masking term and comparison to previous work and photographs. We author each feather manually, by encoding the feathers geometry, including shaft, vane and barb orientation, on a 2D texture on top of a relatively simple geometry. Exploring more effective procedural tools for authoring (e.g., [BP19]) is left as an interesting future research direction.

We implemented our model in Mitsuba 0.6 [Jak10] as a new BSDF. All our renders have been computed on an Intel Core i9-10900KF CPU with 20 cores. Table 2 reports the rendering time of all figures including scene with different complexity in terms of geometry (single feather, feather pelt, feather wing and feather balls), material (brown, black, blue, red and green feathers) and lighting conditions. Since our is surface-based, it is practical in terms of both rendering time and memory for fully feathered assets, which would be very expensive is curve-based feathers.

7.1. Model analysis

We perform ablation studies to analyze the impact of each component of our model. Figure 7 shows how increasing the complexity of the fiber cross section affects the final appearance produced by our fiber BCSDF in a significant manner. As previous work had already shown [KM17], an elliptical cross section with higher eccentricity increases the brightness of the specular lobes (see renders) and introduces new patterns as the elliptical blobs (see latlong reflectance plots). As we introduce a medulla, reflectance distribution gets more uniform and appearance gets smoother. When introducing a non-concentric medulla, reflectance distribution becomes asymmetric and the change in appearance with respect to the concentric case is important, showing a greater variation on appearance with respect to feather orientation.

Figure 8 shows the effect of both our masking and our BCSDF representing feathers, compared against using only hair barbs [LF10, HG19] (first column), and against a more sophisticated feather structure with barbs and barbules modeled with a hair model (second column) and combined with a masking term, similar to the one proposed by Baron and colleagues [BDSP22]. As shown in the four examples, the medulla (third column) is essential to produce softer and non-iridescent structural colors such as green and blue tones. Notice that a closer appearance matching would require to match the lighting conditions and feather geometries more carefully. Nevertheless, the overall appearance produced by our full model better reproduces the real feathers' appearance than previous works.

Finally, in Figure 9 we validate our analytical masking term by comparison against a brute-force 100spp Monte-Carlo simulation of masking over explicit geometry (consisting of 100 barbs with 100 barbules each). Our masking expression yields similar weights to the reference, but without any noise and in constant time.

7.2. Appearance exploration

In Figure 10 we analyze the feather expressivity of our appearance model by exploring the range of appearances that it can achieve. In particular: 1) Increasing the relative barbule separation (δ_{bb}) increases feather transparency as less transmitted rays are blocked by barbules. 2) Increasing barb axis ratio (e_b) increases the frequency of the highlights. Finally, 3) increasing the medulla size changes the hue of the feather, as well as the distribution of reflectance towards a more diffuse one. We provide a more thorough parameter exploration as supplemental material.

7.3. Appearance matching with photographs

We photograph two feathers using a conventional smartphone under different light conditions and create an scene to roughly match lighting conditions, appearance and shape of the captures, while ignoring the plumulaceous regions of the feather. Figure 11 shows our results with the Amazon parrot, demonstrating that our masking can predict the view-dependent changes (top near frontal view, bottom rotated feather) of the final color due to different coloration between green barbs and yellow barbules.

Figure 12 shows a black goose feather lighted from behind. Similar to before, we capture the feather under varying rotation: Without masking, the transparency is independent of the rotation, while our masking predicts the loss on transparency as the feather rotates. In addition, this figure demonstrates again the importance of the medulla to predict the blue tint of the feather due to structural coloration of feathers, which is not physically possible with a hair BCSDF as in previous works.

Note that we do not expect to perfectly match the photographs as they were taken under uncontrolled illumination conditions and the structural and optical parameters of the feather were unknown. In addition, near-field details such as visible individual barbs are not accounted by our model. Still, we show that the combination of our BCSDF and our masking term predict challenging appearance features observed in feathers.

8. Discussion

Far-field vs near-field Our model assumes far-field rendering of feathers, and thus is not able to capture the high-frequency details of visible barbs, which are naturally handled by curve-based methods, which in the far field suffer aliasing. Extending our method to near-field appearance would require more sophisticated authored

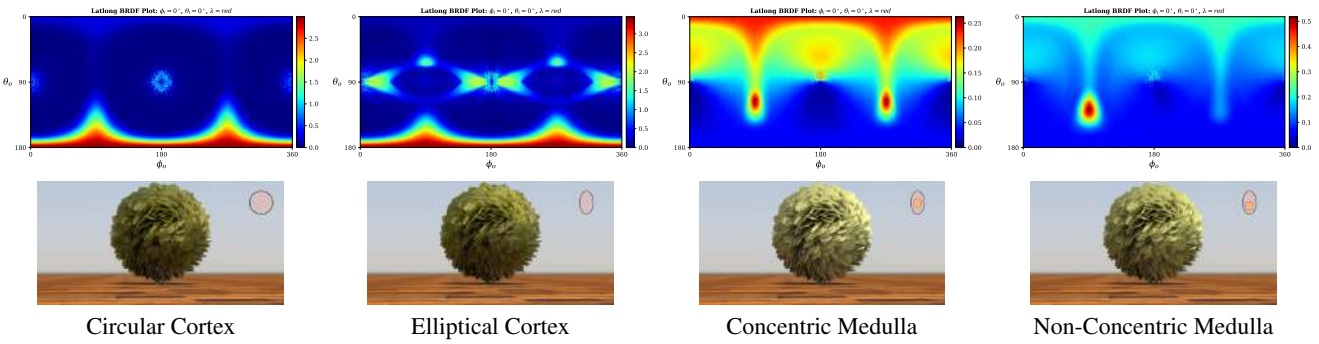

Figure 7: *Ablation studies of the Fiber BCSDF at ($\phi_i = 0º$, $\theta_i = 45º$): single cortex cylinder (first column), elliptical cortex cylinder (second column), nested cylinders with concentric medulla (third column) and nested cylinders with non-concentric medulla (last column). We show the latlong reflectance plots for the red wavelength. Fiber BCSDF parameters: $\sigma_{c,a} = (0.133, 1.967, 2.1)$, $\eta_c = \eta_m = 1.53$, $\beta_m = 0.13$, $\beta_n = 0.12$. The elliptical cross section is $e_b = 1.6$. Medulla is circular with radius 0.6 ($a_m = 0.6, b_m = 0.6$) and the non-concentric medulla is located at $c_x = -0.1$ and $c_y = 0.1$. Latlong reflectance plots are obtained with 10000 spp. Notice how the elliptical cortex increases the reflectance of the render, while the presence of the medulla makes the appearance softer. The latlong reflectance plots also reveals how each component affects the lobe patterns in a significant manner.*

Figure 8: *Ablation studies of our feather BSDF for a feather pelt scene. **[Only hair barbs]:** Only barb with hair BCSDF [MJC*03]; **[Only masking]:** Barb and barbules with Hair BCSDF combined with our masking term similar to [BDSP22]; and **[Full]:** Adding a diffuse medulla inside the Barb BCSDF. Notice how our full model is capable of producing a wide variety of complex appearances that resemble closer the appearance of the photographs than previous works for several birds: From top to bottom, northern cardinal, blue-fronted amazon parrot (we reproduce the blue feathers in the face), eclectus parrot and Brewer's blackbird. In particular, the diffuse reflectance of the medulla is critical to achieve similar tones to the photographs, while the masking is important for goniochromatic and occlusions effects.*

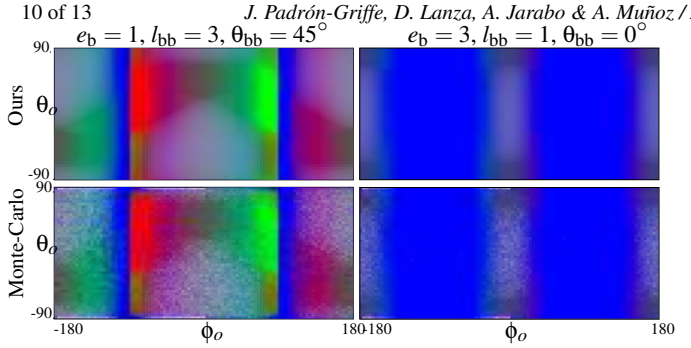

Figure 9: *Comparison between our analytical masking expression (top) and a Monte-Carlo simulation (100spp) with ray tracing towards a full modeled microgeometry for the same parameters (bottom). Two different masking parametrizations have been explored (left and right columns), and the rest of the parameters are the same between the two: $e_{bb} = 1$, $\delta_{bb} = 1$. The horizontal and vertical axes per plot correspond to the view direction ω_o in polar coordinates (θ_o, ϕ_o). The colormap represents the weights of the different microgeometrical components: w_b, w_{bp} and w_{bd} are mapped to the blue, green, and red channels, respectively. Note how our analytical masking expression can obtain a noiseless result in a minimal fraction of the time (constant) while being accurate with respect to a fully modeled microgeometry.*

maps and redefining the masking terms to support per-point masking. Deriving a proper filtering technique for such a near-field model is also left as future work.

Shadowing To simplify our BSDF we decided to omit the shadowing term, which intuitively has little effect in natural lighting conditions. This allows us to use a far-field integration of the BCSDF, instead of requiring integrating both the input and outgoing visible surfaces of the fibers, at the cost of removing some physical plausibility.

Energy conservation Given the lack of shadowing, our BSDF is energy preserving without the need of multiple scattering simulations, except for the potential energy loss in the BCSDF, which might be significant when introducing elliptical cross-sections and an inner scattering medulla. However, as shown in Figure 13, we found that limiting light transport inside the fiber to five lobes result in a minimal energy loss.

Wave optics Our model omits important wave optical behavior, except for the structural coloration of the medulla, which we approximate as a diffuse reflection. Other effects such as the iridescence due to the grating-like structure of barbs and barbules, or the thin-film-like structure in barbules [HMC*22] is omitted. Incorporating these effects, as well as a more principled definition of the medulla's diffuse structural coloration is an interesting avenue for future work.

Other types of feathers An important limitation of our surface-based approach is that is not particularly suitable for plumulaceous feathers, where the vane is not as structured and is therefore more suitable for curve-based representations. Still, our BCSDF could be directly applied to curve-based representations [BDSP22], and hybrid approaches where curve-based barbs encode flyaway and plumulaceous feathers, are probably the best choice for a general model covering the whole spectrum of feather appearances.

Non-elliptical barbs and barbules An additional assumption of our work is the use of elliptical cross sections for barbs and barbules, which is a coarse approximation for both, especially barbules that appear in a large variety of cross sections. We made this choice for limiting the space of parameters of our model into something manageable; however, our methodology for computing the BCSDF based on path tracing is very general, so fibers with arbitrary cross-section could be used, in the same spirit as the work of Aliaga et al. [ACG*17] for cloth fibers.

Parameter space Our model is parametrized by a total of 23 parameters including the masking parameters (5 geometrical parameters), BCSDF barb parameters (12 parameters for cortex and medulla) and BCSDF barbule parameters (6 parameters for the cortex), with absorption coefficients and diffuse reflectance defined by RGB values. The model is expressive as shown in our experiments and the parameter space might seem challenging. However, these parameters all have an intuitive meaning, either structurally or appearance-wise, and the general appearance features of feathers (goniochromatism, view-dependant transmittance, highlights...) emerge naturally. We selected some of the parameter values based on the structural and optical properties observed on feathers in previous works [TWS13, IDS18, MSV*21] and we found the rest empirically. However, targeting a specific feather's appearance required several iterations of parameter editing in our experience. A more example-based automatic parameter selection would definitely be an interesting next step on this research path. Introducing a length-dependent barb radius would probably produce more realistic results.

Conclusion We have presented a practical surface-based far-field appearance model for feathers, in which we model the complex microgeometry of a feather as a light-weight texture and an analytical masking term that accounts for the angular dependent visibility conditions, which previous curve-based models handled explicitly via curve visibility. On the core of our model is a new fiber BCSDF that supports elliptical cross sections and (potentially-colored) scattering medulla, which is crucial for representing a wide variety of real-world feathers.

Acknowledgements

We thank the reviewers for their valuable feedback, Diego Royo and Edurne Bernal for the design of the coloration mechanisms schematic and feather structure sketch respectively, the members of the Graphics and Imaging Lab for proofreading, and CGTrader user *rendyka* for the Amazon Parrot model. This work has been funded by the European Union's Horizon 2020 research and innovation programme under the Marie Skłodowska-Curie grant agreement No 956585 (PRIME).

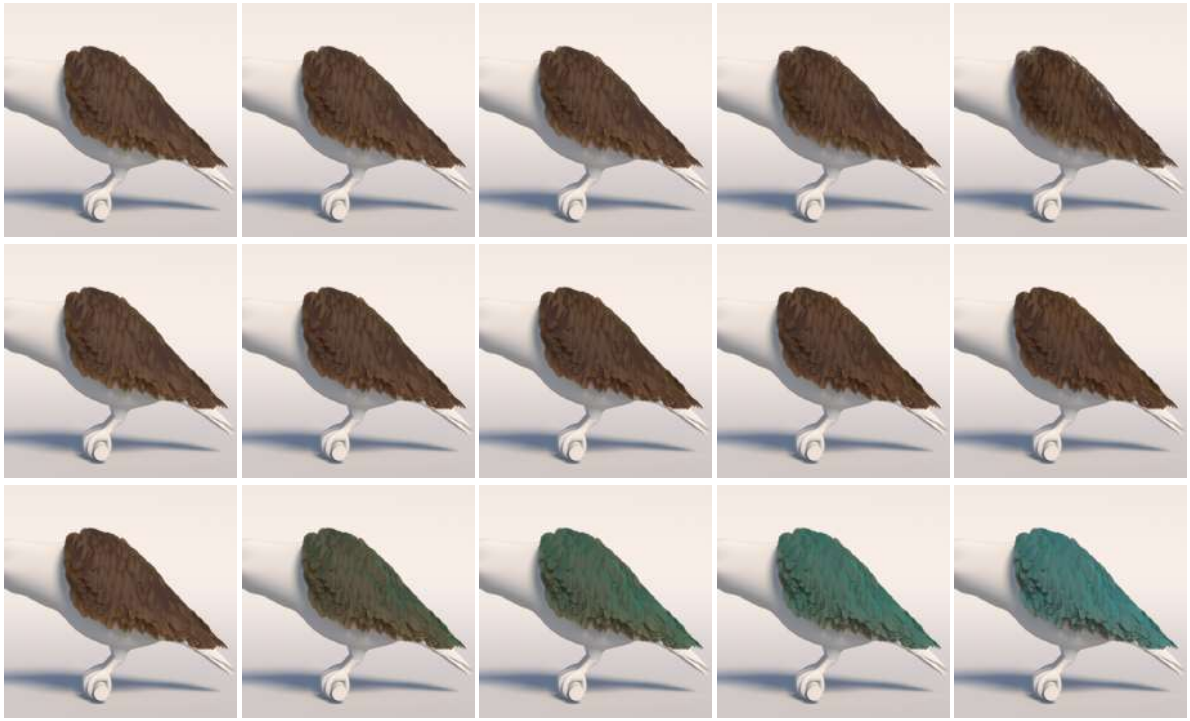

Figure 10: *Parameter exploration of our model.* ***Top:*** *We vary the* $\delta_{bb} = [0.1, 0.3, 0.5, 1.0, 3.0]$. *Larger separation between the barbules increased the transmittance with high values showing prominent transparency effects.* ***Mid:*** *We show the effect of increasing the barb axis ratio* $e_b = [1.0, 1.2, 1.4, 1.6, 1.8]$, *progressively making the central highlight sharper.* ***Bottom:*** *We increase the size of the medulla* $b_m = [0.0, 0.2, 0.4, 0.6, 0.8]$, *for higher values, the color is mostly dominated by the color of the medulla and the appearance becomes more diffuse.*

References

[ACG*17] ALIAGA C., CASTILLO C., GUTIERREZ D., OTADUY M. A., LOPEZ-MORENO J., JARABO A.: An appearance model for textile fibers. *Computer Graphics Forum 36*, 4 (2017). 3, 10

[ANA*20] ANDERSSON P., NILSSON J., AKENINE-MÖLLER T., OSKARSSON M., ÅSTRÖM K., FAIRCHILD M. D.: Flip: A difference evaluator for alternating images. *Proceedings of the ACM on Computer Graphics and Interactive Techniques 3*, 2 (2020), 15:1–15:23. 12

[BDSP22] BARON J., DHILLON D. S., SMITH N. A., PATTERSON E.: Microstructure-based appearance rendering for feathers. *Computers & Graphics 102* (2022), 452–459. 1, 2, 7, 8, 9, 10

[BP19] BARON J., PATTERSON E.: Procedurally Generating Biologically Driven Feathers. *Advances in Computer Graphics 11542* (2019), 342–348. 2, 3, 8

[BP21a] BARON J., PATTERSON E.: Computer-Aided Visual Analysis of Feathers. In *ICPR Workshop on Visual observation and analysis of Vertebrate And Insect Behavior (VAIB)* (2021). 2, 3

[BP21b] BENAMIRA A., PATTANAIK S.: A combined scattering and diffraction model for elliptical hair rendering. *Computer Graphics Forum 40*, 4 (2021), 163–175. 3

[BPMG04] BOSCH C., PUEYO X., MÉRILLOU S., GHAZANFARPOUR D.: A physically-based model for rendering realistic scratches. *Computer Graphics Forum 23*, 3 (2004), 361–370. 3

[CBTB16] CHIANG M. J.-Y., BITTERLI B., TAPPAN C., BURLEY B.: A Practical and Controllable Hair and Fur Model for Production Path Tracing. *Computer Graphics Forum 35*, 2 (2016). 3, 6

[CT81] COOK R. L., TORRANCE K. E.: A reflectance model for computer graphics. *SIGGRAPH Comput. Graph. 15*, 3 (aug 1981), 307–316. 3

[CXGS02] CHEN Y., XU Y., GUO B., SHUM H.-Y.: Modeling and rendering of realistic feathers. *ACM Trans. Graph. 21*, 3 (2002). 2

[d'E21] D'EON E.: An analytic brdf for materials with spherical lambertian scatterers. *Computer Graphics Forum 40*, 4 (2021), 153–161. 3

[dFH*11] D'EON E., FRANÇOIS G., HILL M., LETTERI J., AUBRY J.-M.: An Energy-Conserving Hair Reflectance Model. *Computer Graphics Forum 30* (2011). 2, 3, 5, 6

[DWd*08] DONNER C., WEYRICH T., D'EON E., RAMAMOORTHI R., RUSINKIEWICZ S.: A layered, heterogeneous reflectance model for acquiring and rendering human skin. *ACM Trans. Graph. 27*, 5 (2008). 2

[EHR95] ENNOS A., HICKSON J., ROBERTS A.: Functional morphology of the vanes of the flight feathers of the pigeon columba livia. *The Journal of experimental biology 198*, 5 (1995), 1219–1228. 3

[FS20] FREYER P., STAVENGA D. G.: Biophotonics of diversely coloured peacock tail feathers. *Faraday Discuss. 223* (2020), 49–62. 3

[FWLQ23] FENG L., WANG F., LUO H., QIU B.: Review of recent advancements in the biomimicry of structural colors. *Dyes and Pigments 210* (2023), 111019. 2

[FWS19] FREYER P., WILTS B. D., STAVENGA D. G.: Reflections on iridescent neck and breast feathers of the peacock, pavo cristatus. *Journal of the Royal Society Interface Focus 9*, 1 (2019), 20180043. 4

[HBM13] HARVEY T. A., BOSTWICK K. S., MARSCHNER S.: Directional reflectance and milli-scale feather morphology of the African

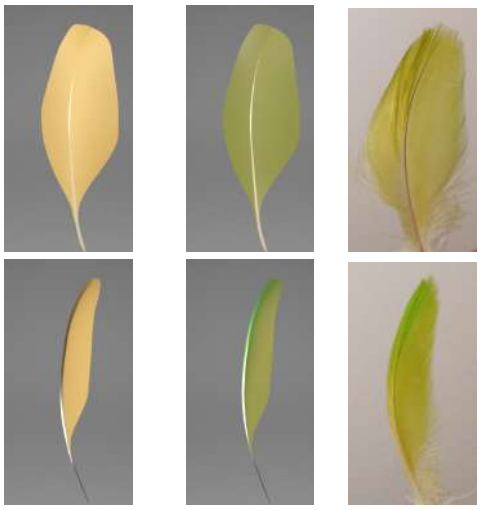

Without masking With masking Photograph

Figure 11: *Qualitative appearance matching on an* Amazon parrot *feather, for a frontal (top) and lateral (bottom) views. As the feather rotates, view dependent changes on the feather's color become apparent: These are produced by visibility changes between barbs (yellow) and barbules (green). Our masking model is roughly able to predict these changes. Please see the supplemental video for a dynamic example of this goniochromism effect.*

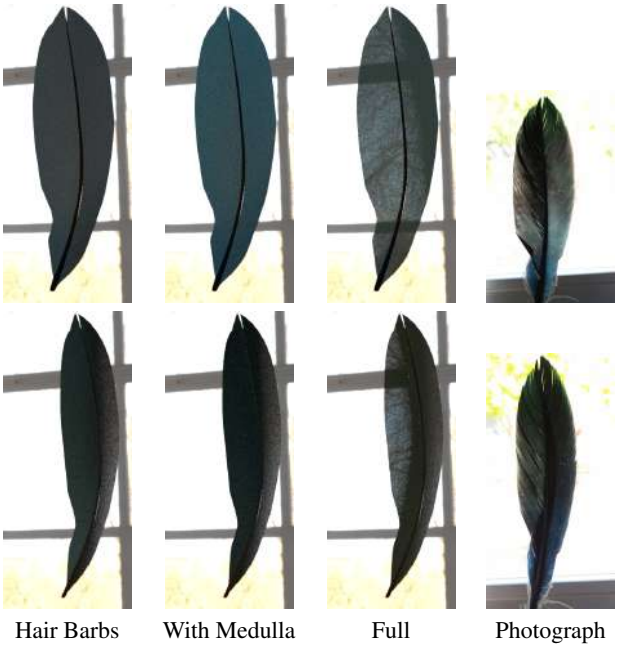

Hair Barbs With Medulla Full Photograph

Figure 12: *Qualitative appearance matching on a* black goose *feather, for a frontal (top) and lateral (bottom) views, under strong back-lighting. Our masking term can reproduce view-dependent transparency. Note that the bluish appearance can only be achieved by the inclusion of a blue medulla.*

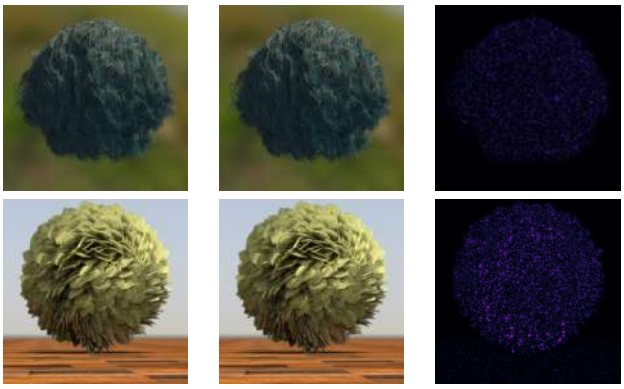

1000 lobes 5 lobes Error

Figure 13: *Energy conservation validation of the BCSDF. For a five-bounces evaluation of our BCSDF we observe minimal differences with respect to a 1000-bounces counterpart, in both fiber-only, single scattering test (top) and inside our feathers BSDF with multiple scattering (bottom). Error is computed using the FLIP metric [ANA*20].*

Emerald Cuckoo, Chrysococcyx cupreus. *Journal of the Royal Society Interface* (2013). 2, 3, 5

[Hei14] HEITZ E.: Understanding the masking-shadowing function in microfacet-based brdfs. *Journal of Computer Graphics Techniques (JCGT) 3*, 2 (June 2014), 48–107. 3

[HG19] HAAPAOJA R., GENZWÜRKER C.: Mesh-driven generation and animation of groomed feathers. In *ACM SIGGRAPH 2019 Talks* (2019). 1, 2, 8

[HHH22] HUANG W., HULLIN M. B., HANIKA J.: A microfacet-based hair scattering model. *Computer Graphics Forum 41*, 4 (2022), 79–91. 3

[HM06a] HILL G. E., MCGRAW K. J.: *Bird coloration: function and evolution*, vol. 2. Harvard University Press, 2006. 1, 2

[HM06b] HILL G. E., MCGRAW K. J.: *Bird coloration: mechanisms and measurements*, vol. 1. Harvard University Press, 2006. 3

[HMC*22] HUANG W., MERZBACH S., CALLENBERG C., STAVENGA D., HULLIN M.: Rendering iridescent rock dove neck feathers. In *ACM SIGGRAPH 2022 Conference Proceedings* (New York, NY, USA, 2022), SIGGRAPH '22, Association for Computing Machinery. 2, 3, 5, 6, 7, 10

[IDS18] IGIC B., D'ALBA L., SHAWKEY M. D.: Fifty shades of white: how white feather brightness differs among species. *The Science of Nature 105*, 3 (2018), 1–15. 3, 10

[IGAJG15] IGLESIAS-GUITIAN J. A., ALIAGA C., JARABO A., GUTIERREZ D.: A biophysically-based model of the optical properties of skin aging. *Computer Graphics Forum 34*, 2 (2015). 2

[IM12] IRAWAN P., MARSCHNER S.: Specular reflection from woven cloth. *ACM Trans. Graph. 31*, 1 (feb 2012). 3

[Jak10] JAKOB W.: Mitsuba renderer. http://mitsuba-renderer.org/, 2010. 8

[JHY*14] JAKOB W., HAŠAN M., YAN L.-Q., RAMAMOORTHI R., MARSCHNER S.: Discrete stochastic microfacet models. *ACM Transactions on Graphics (Proceedings of SIGGRAPH) 33*, 4 (July 2014), 115:1–115:10. 3

[KM17] KHUNGURN P., MARSCHNER S.: Azimuthal scattering from elliptical hair fibers. *ACM Trans. Graph. 36*, 2 (apr 2017). 3, 8

[KZP*24] KHATTAR A., ZHU J., PADOVANI E., AURBY J.-M., DROSKE M., YAN L.-Q., MONTAZERI Z.: A multi-scale yarn appearance model with fiber details. In *Computational Visual Media* (2024). 3

[LF10] LEANING J., FAGNOU D.: Feathers for mystical creatures: creating pegasus for clash of the titans. In *ACM SIGGRAPH 2010 Talks* (2010). 2, 8

[LRPB23] LUCAS S., RIBARDIERE M., PACANOWSKI R., BARLA P.: A micrograin bsdf model for the rendering of porous layers. In *Proceedings of SIGGRAPH Asia 2023* (2023). 3

[MDG00] MÉRILLOU S., DISCHLER J.-M., GHAZANFARPOUR D.: A brdf postprocess to integrate porosity on rendered surfaces. *IEEE Transactions on Visualization and Computer Graphics 6*, 4 (oct 2000), 306–318. 3

[MJC*03] MARSCHNER S. R., JENSEN H. W., CAMMARANO M., WORLEY S., HANRAHAN P.: Light scattering from human hair fibers. *ACM Trans. Graph. 22*, 3 (jul 2003), 780–791. 1, 2, 3, 5, 9

[MPLS*12] MENDES-PINTO M. M., LAFOUNTAIN A. M., STODDARD M. C., PRUM R. O., FRANK H. A., ROBERT B.: Variation in carotenoid–protein interaction in bird feathers produces novel plumage coloration. *Journal of the Royal Society Interface 9*, 77 (2012), 3338–3350. 4

[MSV*21] MCCOY D., SHULTZ A., VIDOUDEZ C., HEIDE E., DALL J., TRAUGER S., HAIG D.: Microstructures amplify carotenoid plumage signals in tanagers. *Scientific Reports 11* (04 2021), 8582. 3, 10

[NLS*10] NOH H., LIEW S. F., SARANATHAN V., MOCHRIE S. G. J., PRUM R. O., DUFRESNE E. R., CAO H.: How noniridescent colors are generated by quasi-ordered structures of bird feathers. *Advanced Materials 22*, 26-27 (2010), 2871–2880. 4, 6

[Pru99] PRUM R. O.: The anatomy and physics of avian structural colours. In *Proc. Int. Ornithol. Congr* (1999), vol. 22, pp. 1633–1653. 4

[PZS*19] PAN Y., ZHENG W., SAWYER R. H., PENNINGTON M. W., ZHENG X., WANG X., WANG M., HU L., CONNOR J., ZHAO T., LI Z., SCHROETER E. R., WU F., XU X., ZHOU Z., SCHWEITZER M. H.: The molecular evolution of feathers with direct evidence from fossils. *Proceedings of the National Academy of Sciences 116*, 8 (2019), 3018–3023. 3

[RPD*14] RIEDLER R., PESME C., DRUZIK J., GLEESON M., PEARLSTEIN E.: A review of color-producing mechanisms in feathers and their influence on preventive conservation strategies. *Journal of the American Institute for Conservation 53*, 1 (2014), 44–65. 3, 4

[SBDDJ13] SADEGHI I., BISKER O., DE DEKEN J., JENSEN H. W.: A Practical Microcylinder Appearance Model for Cloth Rendering. *ACM Trans. Graph. 32*, 2 (April 2013). 3

[SD17] SHAWKEY M. D., D'ALBA L.: Interactions between colour-producing mechanisms and their effects on the integumentary colour palette. *Philosophical Transactions of the Royal Society B: Biological Sciences 372*, 1724 (2017), 20160536. 4

[SH02] STREIT L., HEIDRICH W.: A biologically-parameterized feather model. *Computer Graphics Forum 21*, 3 (2002), 565–573. 3

[SLMO11] STAVENGA D. G., LEERTOUWER H. L., MARSHALL N. J., OSORIO D.: Dramatic colour changes in a bird of paradise caused by uniquely structured breast feather barbules. *Proceedings of the Royal Society B: Biological Sciences 278*, 1715 (2011), 2098–2104. 3

[Sta01] STAM J.: An illumination model for a skin layer bounded by rough surfaces. In *Rendering Techniques 2001*. Springer, 2001, pp. 39–52. 2

[STLW11] STAVENGA D. G., TINBERGEN J., LEERTOUWER H. L., WILTS B. D.: Kingfisher feathers – colouration by pigments, spongy nanostructures and thin films. *Journal of Experimental Biology 214*, 23 (12 2011), 3960–3967. 4

[Str03] STREIT L. M.: *Modelling of Feather Coat Morphogenesis for Computer Graphics*. PhD thesis, 2003. 2

[SWEM17] SULLIVAN T. N., WANG B., ESPINOSA H. D., MEYERS M. A.: Extreme lightweight structures: avian feathers and bones. *Materials Today 20*, 7 (2017), 377–391. 3

[TWS13] TINBERGEN J., WILTS B. D., STAVENGA D. G.: Spectral tuning of Amazon parrot feather coloration by psittacofulvin pigments and spongy structures. *Journal of Experimental Biology 216*, 23 (12 2013), 4358–4364. 10

[Vea97] VEACH E.: *Robust Monte Carlo Methods for Light Transport Simulation*, vol. 1610. Stanford University PhD thesis, 1997. 5

[WDM*12] WALSH N., DALE J., MCGRAW K. J., POINTER M., MUNDY N. I.: Candidate genes for carotenoid coloration in vertebrates and their expression profiles in the carotenoid-containing plumage and bill of a wild bird. *Proceedings of the Royal Society B: Biological Sciences 279*, 1726 (2012), 58–66. 4

[WMLT07] WALTER B., MARSCHNER S. R., LI H., TORRANCE K. E.: Microfacet models for refraction through rough surfaces. In *Proceedings of EGSR* (2007), p. 195–206. 3

[XWM*20] XIA M. M., WALTER B., MICHIELSSEN E., BINDEL D., MARSCHNER S.: A wave optics based fiber scattering model. *ACM Trans. Graph. 39*, 6 (nov 2020). 3

[YJR17] YAN L.-Q., JENSEN H. W., RAMAMOORTHI R.: An Efficient and Practical near and Far Field Fur Reflectance Model. *ACM Trans. Graph. 36*, 4 (2017). 3

[YTJR15] YAN L.-Q., TSENG C.-W., JENSEN H. W., RAMAMOORTHI R.: Physically-accurate fur reflectance: Modeling, measurement and rendering. *ACM Trans. Graph. 34*, 6 (oct 2015). 2, 3, 5

[ZK20] ZHANG J., KANAI T.: Biological modeling of feathers by morphogenesis simulation. In *2020 International Conference on Cyberworlds (CW)* (2020), pp. 63–70. 2

[ZKO*10] ZHANG F., KEARNS S., ORR P., BENTON M., ZHOU Z., JOHNSON D., XU X., WANG X.: Fossilized melanosomes and the colour of cretaceous dinosaurs and birds. *Nature 463* (02 2010), 1075–8. 2

[ZW07] ZINKE A., WEBER A.: Light scattering from filaments. *IEEE Transactions on Visualization and Computer Graphics 13*, 2 (2007), 342–356. 4

[ZZW*22] ZHU J., ZHAO S., WANG L., XU Y., YAN L.-Q.: Practical level-of-detail aggregation of fur appearance. *ACM Trans. Graph. 41*, 4 (2022). 3